Nonequilibrium Oscillatory Electron Transfer in Bacterial Photosynthesis

Koji Ando*,†,§ and Hitoshi Sumi*,‡,§

Institute of Materials Science, University of Tsukuba, Tsukuba, Ibaraki 305-8573, Japan

Received: June 17, 1998; In Final Form: September 25, 1998

A theory to describe nonequilibrium electronic surface crossing during vibrational relaxation induced by ultrafast photoexcitation is developed and applied to the primary electron transfer (ET) in bacterial photosynthetic reaction centers. As a key concept, we define on a microscopic basis the angle between two reaction coordinates each representing the environmental nuclear displacements coupled to the initial photoexcitation (to the P* state) and to the subsequent ET processes, respectively. The "cross-spectral" density function, whose integral intensity gives the cosine of this angle, is also defined to give a consistent (nonphenomenological) description of the vibrational coherence and its dephasing. In the application to the primary ET in bacterial photosynthesis, we find (1) the time-dependent ET rate exhibits marked oscillation at low temperatures due to the nonequilibrium vibrational coherence in the P* state. However, it does not contribute very much to accelerate the primary ET rate with respect to the total population decay of the P* state. (2) The static energetics (that give a small barrier for the ET) and the nuclear quantum tunneling effect at low temperatures, rather than the dynamical nuclear coherence, are the main origins that reasonably reproduce the ultrafast ET and its anomalous temperature dependence (accelerated as the temperature decreases). From the calculations on alternative parameter regimes, we also examine the conditions in which the nonequilibrium nuclear vibrations may accelerate the photoinduced ET. We further propose that detailed experimental analysis of the transient behavior of the oscillating time-dependent reaction rate may provide useful information on the interplay between the vibrational dephasing and the surface crossing dynamics of ultrafast reactions as well as on the underlying static energetics of the system.

I. Introduction

The primary electron transfer (ET) in the reaction centers (RCs) of photosynthetic purple bacteria (*Rhodobacter sphaeroides* and *Rhodopseudomonas viridis*) takes place from the photoexcited bacteriochlorophyll special pair P* to the bacteriopheophytin H_L in ∼3 ps at 300 K,[1,2] possibly involving a transfer to the accessory bacteriochlorophyll B_L located between P and H_L as a real or virtual intermediate state. During this extraordinarily fast reaction, the protein environment may not be thermally relaxed. Moreover, as this process accelerates at lower temperature (∼1 ps at 10 K),[3] the nonequilibrium situation may become more significant. Indeed, it has been observed recently that the time-resolved stimulated[4] and spontaneous[5] emission from the P* state exhibits quantum beat (coherence) for a few picoseconds with ∼450 fs period. The corresponding vibrational frequency was also observed by resonance Raman scattering[6] and hole-burning spectroscopies.[7]

In order to fully describe the competition between the ET and the environmental relaxation, we apparently need to go beyond the thermal equilibrium assumption of the standard theories. It is also desirable to develop a theory which is simple enough to be useful for experimental analyses and for our conceptual understanding.

The observation of nuclear vibrational coherence accompanying electronic relaxation is becoming commonplace owing to the recent development of the ultrafast spectroscopic techniques.[8] Photosynthetic light-harvesting antenna[9] and rhodopsin retinal[10] are other photobiological systems in which coherent vibrational motions have been observed. Vibrational quantum beats are also seen in nonbiological condensed-phase chemical systems which involve electronic curve crossing processes.[11]

Motivated by these novel experimental findings, a number of theoretical studies have emerged in these years[12−19] and have provided intriguing clues for understanding the basic aspects of the nonequilibrium nuclear coherence effects. However, many of them are restricted to models of one-dimensional reaction coordinates perturbatively coupled to heat baths. Consequently, as pointed in the following, some fundamental aspects of the real systems (especially the heterogeneity of the protein environment which appears essential for the bacterial photosynthetic ET) do not seem to have been fully addressed.

First we note that the initial photoexcitation and the subsequent curve-crossing processes generally involve different couplings to the (environmental) nuclear displacements from each other. This would be particularly the case for the bacterial photosynthetic RCs due to the heterogeneity of the protein environment around the embedded chromophores. That is, the photoexcitation to P* mainly involves the displacements of the protein around P (and of P itself), while the subsequent ET couples to the protein around both P and the electron acceptor(s) B_L and/or H_L. (Even locally, the magnitude and the direction of the nuclear displacements interacting with P* and P^+ ion would be different).

To take account of this aspect, we start with a model[20,21] of an infinite number of bath modes coupled to the photoexcitation and the ET each with an *arbitrary* spectral density. From this

† E-mail: ando@ims.tsukuba.ac.jp.
‡ E-mail: sumi@ims.tsukuba.ac.jp.
§ Fax: 81(Japan)-298-7440.

10.1021/jp982659l CCC: $15.00
Published on Web 12/08/1998

we define (or extract) two reaction coordinates for each of these processes and the *angle* between them. A time-dependent ET rate formula is then derived as a function of this angle. The vibrational coherence and its dephasing are consistently described on a nonphenomenological microscopic basis. For example, the theory naturally includes a limit where the two reaction coordinates are orthogonal to each other, in which the nuclear coherence observed in the P* state wound not be actually relevant to the ET process.

Among the previous works, a recent one by Cho and Silbey[17] seems to be most closely related to the present study (though the bacterial photosynthetic ET was not examined there). Another related work to be mentioned is the one by Kharkats et al.[18] which explicitly considers the bacterial RCs. Comparison between these and our theory will be sketched in section II.

While the main result of the present formulation includes arbitrary bath spectral densities, we also derive a simplified rate formula described by a small set of parameters such as the characteristic frequencies and the reorganization energies of the environment. We remark this would be also useful for experimental analyses. It is then employed for the numerical application to the bacterial photosynthetic primary ET with the parameters obtained from currently available experimental information. The possible impact of the nuclear coherence in P* state on the primary ET rate and mechanism is explored as a function of the angle between the two reaction coordinates. The origin of the anomalous temperature dependence of the primary ET rate is also discussed. Finally, we propose that detailed spectroscopic analysis of the short time oscillatory behavior of the time-dependent ET rate could provide a useful key for elucidating the dynamical mechanisms and the underlying static energetics of ultrafast reactions.

Section II describes the theoretical model. Numerical calculations with the parameters for the bacterial photosynthetic RCs are presented in section III. Alternative parameter regimes are also examined in order to illuminate the essential features of the photosynthetic systems. Section IV summarizes and concludes the paper.

II. Theory

The theory described here is applicable for general nonequilibrium surface crossing processes induced by ultrafast photoexcitations. However, it would be convenient (and enough) to present it rather specifically for the primary ET in bacterial photosynthesis.

Here we restrict our study to the ET from the special pair P to the accessory bacteriochlorophyll B_L rather than to the bacteriopheophytin H_L. This implies that we are assuming dominance of the sequential (stepwise) mechanism, $P^* \rightarrow P^+B_L^- \rightarrow P^+H_L^-$. As shown in refs 22 and 23, the "sequential" and "superexchange" mechanisms are mutually opposite limits of a unified single process. (This is theoretically isomorphic with the resonance Raman scattering in the second order optical processes.) The numerical calculations by the unified theory in ref 23 have demonstrated that the bacterial primary ET rate is basically determined by the ET step from P to B_L. We also note that the recent experimental analysis by Schmidt et al.[24] supports the sequential mechanism.

We start with a harmonic bath model for the electronically diabatic (phonon) Hamiltonians for the ground (PB_L, H_1), locally excited (P^*B_L, H_2), and charge transfer ($P^+B_L^-$, H_3) states, where

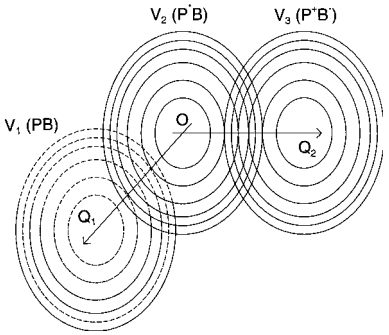

Figure 1. Schematic drawing of the diabatic potential energy surfaces of the ground (PB_L; V_1), locally excited (P^*B_L; V_2), and charge transfer ($P^+B_L^-$; V_3) states. The reaction coordinates Q_1 and Q_2 represent the nuclear displacements coupled to the photoexcitation and the electron transfer processes, respectively.

$$H_1 = K + \sum_i \frac{\hbar\omega_i}{2}\left(x_i - \frac{\xi_i}{\hbar\omega_i}\right)^2 + \sum_j \frac{\hbar\omega_i}{2} y_j^2 + \epsilon_1$$

$$H_2 = K + \sum_i \frac{\hbar\omega_i}{2} x_i^2 + \sum_j \frac{\hbar\omega_j}{2} y_j^2$$

$$H_3 = K + \sum_i \frac{\hbar\omega_i}{2}\left(x_i - \frac{\xi'_i}{\hbar\omega_i}\right)^2 + \sum_j \frac{\hbar\omega_j}{2}\left(y_j - \frac{\eta_j}{\hbar\omega_j}\right)^2 + \epsilon_3 \quad (1)$$

$K = \sum_i (\hbar\omega_i/2)p_i^2 + \sum_j (\hbar\omega_j/2)p_j^2$ denotes the kinetic energy. (x_i, p_i) and (y_j, p_j) are the dimensionless coordinates and conjugate momenta representing the bath modes around P and B_L, respectively, satisfying the commutation relation $[x_i, p_{i'}] = i\delta_{i,i'}$ and $[y_j, p_{j'}] = i\delta_{j,j'}$. [Here, the division into the $\{x_i\}$ and $\{y_j\}$ sets is made specifically for the bacterial RCs. Modification of the final formulas for more general situations is very straightforward.] We omit the displacements of the $\{y_i\}$ modes in H_1 and H_2 because these describe the bath couplings around B_L that are expected to be minor in the photoexcitation of P. [As noted above, the inclusion of $\{y_j\}$ is straightforward if needed.] The energy differences of the potential minima for H_1 and H_3 from H_2 are denoted by ϵ_1 and ϵ_3, respectively.

A schematic drawing of the model is displayed in Figure 1. We define the reaction coordinates Q_1 and Q_2 for the photoexcitation and the ET processes by

$$Q_1 \equiv \sum_i \xi_i x_i$$

$$Q_2 \equiv \sum_i \xi'_i x_i + \sum_j \eta_j y_j \quad (2)$$

With this definition, the surface-crossing condition for the ET (in the semiclassical approximation), $H_2 - H_3 = 0$, is written as

$$Q_2 = \lambda'_x + \lambda_y + \epsilon_3 \qquad (\equiv\Delta) \quad (3)$$

where λ'_x and λ_y are the reorganization energies of the $\{x_i\}$ and

$\{y_j\}$ baths associated with the ET, given by

$$\lambda'_x = \sum_i \frac{\xi_i'^2}{2\hbar\omega_i}, \quad \lambda_y = \sum_j \frac{\eta_j^2}{2\hbar\omega_j} \tag{4}$$

In the same way, the reorganization energy for the photoexcitation process is $\lambda_x = \sum \xi_i^2/2\hbar\omega_i$.

The time evolution of the coordinate Q_2 in the P*B_L state, described by $Q_2(t) = e^{iH_2t/\hbar}Q_2e^{-iH_2t/\hbar}$, can be expressed as

$$\begin{aligned} Q_2(t) &= \sum_i \xi'_i x_i(t) + \sum_j \eta_j y_j(t) \\ &= \sum_i \xi'_i(x_i \cos \omega_i t + p_i \sin \omega_i t) + \sum_j \eta_j(y_j \cos \omega_j t + \\ &\qquad p_j \sin \omega_j t) \\ &\equiv Q_{2x}(t) + Q_{2y}(t) \end{aligned} \tag{5}$$

in which $x_i = x_i(0)$, $p_i = p_i(0)$, and so on.

Under the condition $\hbar\omega_{i,j} \ll \lambda'_x + \lambda_y$ that applies for the present system, the bath modes can be treated semiclassically so that the variables $\{x_i, p_i\}$, etc., are regarded as *c*-numbers.[20] The time evolution of $Q_2(t)$ as eq 5 is then given for each initial condiiton $\{x_i, p_i\}$, and the final average over its ensemble determines the time-dependent ET rate.

Now we consider the situation in which the system is initially in thermal equilibrium in the ground state at $t < 0$ and then photoexcited to the locally excited state at $t = 0$ with ultrashort (i.e., broad energy) laser pulse. In this case, the ensemble of $\{x_i, p_i\}$, etc., has a weight determined by the Wigner distribution function[25]

$$\prod_{i,j} W\left(p_i, x_i - \frac{\xi_i}{\hbar\omega_i}\right) W(p_j, y_j) \tag{6}$$

for the thermal equilibrium at $t < 0$. By taking the ensemble average of the ET flux determined from the evolutions of $Q_2(t)$ as described above, the time-dependent ET rate is expressed as

$$k_{ET}(t) = \langle\langle \delta(Q_2(t) - \Delta)\kappa(\dot{Q}_2(t))|\dot{Q}_2(t)|\rangle\rangle_1 \tag{7}$$

which is viewed as a nonequilibrium extension of the ET rate in the semiclassical approximation. The double bracket in eq 7 is defined by

$$\langle\langle ... \rangle\rangle_1 = \prod_{i,j} \int\int dx_i\, dp_i\, dy_j\, dp_j ... W\left(p_i, x_i - \frac{\xi_i}{\hbar\omega_i}\right) W(p_j, y_j) \tag{8}$$

We employ the following form for the transmission coefficient κ at the crossing

$$\kappa(\dot{Q}) \equiv P_{LZ}(|\dot{Q}|)\theta(\dot{Q}) + \frac{P_{LZ}(|\dot{Q}|)}{1 + P_{LZ}(|\dot{Q}|)} \tag{9}$$

in which $\theta(x)$ is the Heaviside step function. (An explanation of this form is given in Appendix A). P_{LZ} is the transition probability per crossing, for which we assume the following Landau−Zener form[20,26]

$$P_{LZ}(|\dot{Q}|) = 1 - \exp\left(-\frac{2\pi J^2}{\hbar|\dot{Q}|}\right) \tag{10}$$

where J is the electronic coupling for the ET.

Because the Wigner distribution function of harmonic systems has a Gaussian form,[25] the integration for the coordinates $\{x_i\}$ and $\{y_i\}$ can be done rather straightforwardly. Also, the many-dimensional integration for the momenta $\{p_i\}$ and $\{p_j\}$ can be reduced to a single integral. As outlined in Appendix B, the final formula is thus derived as

$$k_{ET}(t) = F_Q(t)F_P(t)$$

in which

$$F_Q(t) = \sqrt{\frac{1}{\pi\Lambda}} \exp\left[-\frac{(\bar{Q}_{2x}(t) - \Delta)^2}{\Lambda}\right] \tag{11}$$

$$F_P(t) = \sqrt{\frac{1}{\pi\Gamma}} \int_{-\infty}^{\infty} dP\, e^{-P^2/\Gamma}\, \kappa(\dot{\bar{Q}}_{2x}(t) + P)\, |\ddot{\bar{Q}}_{2x}(t) + P|$$

$$\bar{Q}_{2x}(t) = \sum_i \frac{\xi_i\xi'_i}{\hbar\omega_i} \cos \omega_i t \tag{12}$$

and

$$\begin{aligned} \Lambda &= \sum_i \xi_i'^2 \coth\left(\frac{\beta\hbar\omega_i}{2}\right) + \sum_j \eta_j^2 \coth\left(\frac{\beta\hbar\omega_j}{2}\right) \\ \Gamma &= \sum_i \xi_i'^2\omega_i^2 \coth\left(\frac{\beta\hbar\omega_i}{2}\right) + \sum_j \eta_j^2\omega_j^2 \coth\left(\frac{\beta\hbar\omega_j}{2}\right) \end{aligned} \tag{13}$$

As explained in Appendix B, $\bar{Q}_{2x}(t)$ represents the "average" or the "systematic part" of the nonequilibrium evolution of the Q_{2x} coordinate, from which the thermally fluctuating component has been subtracted to be integrated out. In other words, $\bar{Q}_{2x}(t)$ represents the temperature independent component of the vibrational coherence and its dephasing (projected onto the ET coordinate Q_2) that originates directly from the nonequilibrium displacements created at $t = 0$.

$F_Q(t)$ represents the probability distribution of the surface crossings due to the thermal fluctuation around $\bar{Q}_{2x}(t)$. Indeed, $F_Q(t)$ comes from the δ function of the surface crossing condition in eq 7 which is broadened by averaging over the thermal distribution of the bath coordinates. On the other hand, $F_P(t)$ represents the transmission flux coming from the thermal average of the ET probability at each crossing that is determined by the fluctuation around $\dot{\bar{Q}}_{2x}(t)$.

The coupling coefficients and the (Boltzmann) temperature $k_BT(\equiv\beta^{-1})$ are included in eq 11 via Λ and Γ, which represent the widths of the fluctuation of the reaction coordinate $Q_2(t)$ around its average motion $\bar{Q}_{2x}(t)$ and the velocity $\dot{Q}_2(t)$ around its average motion $\dot{\bar{Q}}_{2x}(t)$, respectively. Their meaning would become clearer by taking the classical limit $\beta\hbar\omega \to 0$

$$\begin{aligned} \Lambda &\to 4k_BT(\lambda'_x + \lambda_y) \\ \Gamma &\to 4k_BT(n'_x\omega'^2_x\lambda'_x + n_y\omega_y^2\lambda_y) \end{aligned} \tag{14}$$

in which, for example, ω_y is the characteristic frequency of the $\{y_i\}$ bath mode and n_y is a number of order unity determined from the functional form of the spectral density.

Now we introduce a "cross-spectral" density function defined by

$$c(\omega) \equiv \sum_i \frac{\xi_i \xi_i'}{2\hbar} \delta(\omega - \omega_i) \tag{15}$$

and rewrite $\bar{Q}_{2x}(t)$ as

$$\bar{Q}_{2x}(t) = \int_0^\infty d\omega \frac{2c(\omega)}{\omega} \cos \omega t \tag{16}$$

The evolution of $\bar{Q}_{2x}(t)$ exhibits under- or overdamped oscillation according to the frequency dispersion of c(ω). (See Appendix C.)

If the cross term $\xi_i\xi_i'$ in eq 15 is replaced by diagonal terms, ξ_i^2, $\xi_i'^2$, or η_j^2, the "ordinary" spectral density functions for the bath coupling, denoted here by $\rho_x(\omega)$, $\rho_{x'}(\omega)$, or $\rho_y(\omega)$, are obtained. For example, $\rho_x(\omega) \equiv \sum_i \xi_i^2 \delta(\omega - \omega_i)/2\hbar$ represents the coupling of the $\{x_i\}$ bath modes to the photoexcitation and is connected to the reorganization energy via $\lambda_x = \int d\omega \rho_x(\omega)/\omega$. Also, Λ and Γ defined in eq 13 can be expressed in terms of these ordinary spectral density functions.

Similarly to the ordinary reorganization energies, we define a quantity λ_c related to c(ω) by

$$\lambda_c \equiv \int_0^\infty d\omega \frac{c(\omega)}{\omega} = \sum_i \frac{\xi_i \xi_i'}{2\hbar\omega_i} \tag{17}$$

This has a form of a scalar product of vectors defined by $\mathbf{v} \equiv \{\{\xi_i/\sqrt{2\hbar\omega_i}\}, 0\}$ and $\mathbf{u} \equiv \{\{\xi_i'/\sqrt{2\hbar\omega_i}\}, \{\eta_j/\sqrt{2\hbar\omega_j}\}\}$. From these we define an angle θ via

$$\cos\theta \equiv \frac{\lambda_c}{\sqrt{\lambda_x(\lambda_x' + \lambda_y)}} \left(= \frac{\mathbf{v}\cdot\mathbf{u}}{|\mathbf{v}||\mathbf{u}|}\right) \tag{18}$$

Because **v** and **u** consist of the (frequency-weighted) bath coupling coefficients for the photoexcitation and the ET processes, respectively, θ is regarded as the angle between the reaction coordinates Q_1 and Q_2.

The magnitude of $\bar{Q}_{2x}(t)$, which is closely connected to λ_c, can be conveniently specified by the parameters λ_x, λ_x', λ_y, and θ. As illustrated in the following sections, this angle θ is a key quantity, both practical and conceptual, for understanding the vibrational coherence and dephasing effects on the ultrafast nonequilibrium surface-crossing rates and mechanisms.

Because of the frequency dispersion of the bath modes $\bar{Q}_{2x}(t)$ decays to zero as $t \to \infty$. Even in this limit, the thermally fluctuating component that has been subtracted from $Q_{2x}(t)$ remains nonvanishing (having width Λ) and gives a finite steady state rate $k_{ET}(\infty)$. (See Appendix B.)

It is intriguing to note here that the perturbational (i.e., nonadiabatic, small J) limit of eq 11, where

$$k_{ET}(t) \to \frac{2J^2}{\hbar} \sqrt{\frac{\pi}{\Lambda}} \exp\left[-\frac{(\bar{Q}_{2x}(t) - \Delta)^2}{\Lambda}\right] \tag{19}$$

is essentially equivalent to eq 28 of ref 17 by Cho and Silbey derived via a quite different route (with a perturbational approach from the beginning).[27] However, the underlying intrinsic assumption of the perturbational limit is (sufficiently) small reaction probability at each surface crossing. In this limit, therefore, the major portion of the ET is rather expected to occur after completion of the thermalization of the reaction coordinate, and thus the steady-state reaction kinetics would be most adequate under this assumption.

In ref 18 Kharkats et al. examined the time evolution of the locally excited P* state after ultrafast photoexcitation in a many-dimensional potential model, for which they derived a formula somehow similar to $F_Q(t)$ in eq 11. Although they considered the Landau-Zener factors for the primary ET in a separate argument, no explicit formula for the time-dependent ET rate corresponding to eq 11 or eq 19 was given.[28]

III. Numerical Results

In order to evaluate $k_{ET}(t)$ and $\bar{Q}_{2x}(t)$ for specific systems, the parameters Λ, Γ, Δ, and the cross-spectral density function $c(\omega)$ are needed. Equivalently, ϵ_3 and the functions $\rho_x(\omega)$, $\rho_{x'}(\omega)$, $\rho_y(\omega)$, and $c(\omega)$ provide the complete information.

These might be evaluated by various experimental (thermochemical and spectroscopic) analyses. However, the evaluation of c(ω) would be particularly a nontrivial task. Alternatively, molecular dynamics (MD) simulations could provide full (or complementary) information for realistic molecular models. Instead, we introduce here a few simplifying approximations to eq 11 and perform numerical calculations by making use of information currently available from the literature.

We first approximate Λ and Γ of eq 13 as

$$\Lambda \simeq 2\hbar \left[\Omega_x'\lambda_x' \coth\left(\frac{\beta\hbar\Omega_x'}{2}\right) + \Omega_y\lambda_y \coth\left(\frac{\beta\hbar\Omega_y}{2}\right)\right]$$

$$\Gamma \simeq 2\hbar \left[\Omega_x'^3\lambda_x' \coth\left(\frac{\beta\hbar\Omega_x'}{2}\right) + \Omega_y^3\lambda_y \coth\left(\frac{\beta\hbar\Omega_y}{2}\right)\right] \tag{20}$$

Namely, the bath contributions are represented by their characteristic frequencies Ω_x' and Ω_y and reorganization energies. (Obviously, it is very straightforward to extend eq 20 to include three or more representative bath contributions.) It is seen that with this approximation the explicit functional forms of the ordinary spectral densities $\rho_x(\omega)$, etc., are no longer necessary.

Next we assume the following form for the cross-spectral density:

$$c(\omega) = A\omega^3 \sqrt{\omega_c^2 - \omega^2} \qquad (0 \le \omega \le \omega_c) \tag{21}$$

The prefactor A is determined from the sum relation eq 17 to be $A = 16\lambda_c/\pi\omega_c^4$. This $c(\omega)$ is "superohmic", $c(\omega) \sim \omega^s$ with $s = 3 > 1$ at $\omega \sim 0$, and is truncated at $\omega = \omega_c$. This form is chosen here for the following reasons: (1) we consider that the truncated form would be realistic for the spectral density of molecular systems compared to the long-tailed exponential cutoff. Indeed, MD simulations of ETs in polar liquid solvents[29] have demonstrated that the calculated spectral densities are well described by the truncated form. (2) On the other hand, because the bacterial photosynthetic RCs have rather rigid structures compared to fluids, it would be adequate (and useful) to refer to the extensively studied polaron problem, for which the coupling to an acoustic photon bath in the low ω limit was shown[30] to be superohmic with $s = 3$ or 5. Additional considerations on the functional form of $c(\omega)$ are given in Appendix C.

By putting eq 21 into eq 16, $\bar{Q}_{2x}(t)$ and its velocity $\dot{\bar{Q}}_{2x}(t)$ are calculated analytically as

$$\bar{Q}_{2x}(t) = \frac{16\lambda_c}{(\omega_c t)^2}\{\omega_c t J_1(\omega_c t) - 3J_2(\omega_c t)\}$$

$$\dot{\bar{Q}}_{2x}(t) = -\frac{16\lambda_c\omega_c}{(\omega_c t)^2}\{\omega_c t J_2(\omega_c t) - 3J_3(\omega_c t)\} \qquad (22)$$

in which $J_n(x)$ denotes the nth order Bessel function.

In the followings, eqs 20 and 22 are employed for the numerical calculations. It would be also worth pointing here that this simplified version of the theory is expected to be useful for experimental analyses, too.

A. Primary ET in Bacterial Photosynthesis. With the approximations introduced above, the necessary parameters to compute $k_{ET}(t)$ are reduced to ϵ_3, λ'_x, λ_y, Ω'_x, Ω_y, ω_c, λ_c, and the electronic coupling J. We determine λ_c from λ_x, λ'_x, λ_y, and θ via eq 18. Practically, it is not necessary to separate λ'_x and λ_y here since they always appear as a sum $\lambda'_x + \lambda_y$. The parameters (except for J and θ) are basically taken from experimental studies on *Rhodobacter sphaeroides.*

We employ $\epsilon_3 = -500$ cm^{-1} and $\lambda_x = 240$ cm^{-1} by referring to experimental analyses by Schmidt et al.[24] (in which they actually proposed $\epsilon_3 = -450$ cm^{-1}) and by Lyle et al.,[7] respectively. Both the resonance Raman[6] and the hole-burning[7] experiments have shown that the dominant bath frequency coupled to P → P* excitation is around 120 cm^{-1}, which we employ for Ω_x. We also assume $\Omega'_x = \Omega_x$ as both of them are associated with the $\{x_i\}$ bath modes. Since we have no direct information on Ω_y, we put rather arbitrarily $\Omega_y = \Omega_x$.[31]

The electronic coupling J is taken to be 35 cm^{-1}, which has been employed in ref 23 by referring to semiempirical (extended Hückel[32] and INDO[33]) molecular orbital calculations and shown to give adequate (static) primary ET rate. It has been also shown in ref 23 that $\lambda'_x + \lambda_y = 700$ cm^{-1} provides reasonable results, which we employ here.

The cutoff frequency ω_c is determined as follows. First, it is seen from the definition eq 15 that $c(\omega)$ is connected to the $\{x_i\}$ bath modes via the coupling coefficients $\{x_i\}$ and $\{x'_i\}$. Thus we determine ω_c from Ω_x (=Ω'_x here) and $c(\omega)$ by

$$\Omega_x \simeq \int_0^{\omega_c} d\omega\ \omega c(\omega) / \int_0^{\omega_c} d\omega\ c(\omega) \qquad (23)$$

which gives $\omega_c = (64/15\pi)\Omega_x$ for $c(\omega)$ of eq 21.

Since we have no clue at present for evaluating θ (or equivalently λ_c) for the bacterial RCs, we examine the rate and the mechanism of the primary ET as a function of θ.

Figure 2 shows the computed $k_{ET}(t)$ for cos $\theta = 0$, -0.5, and -1 at $T = 300$ K and 10 K. It is seen that the oscillation of $k_{ET}(t)$ is remarkable at the low temperature and for the "linear" arrangement (cos $\theta = -1$) of the two reaction coordinates. For the "orthogonal" arrangement, cos $\theta = 0$, $k_{ET}(t)$ is constant. It is noteworthy that the oscillation period is about ~0.1 ps in the very early stage within ~0.3 ps and then changes to ~0.2 ps (almost double) in the longer time. As discussed in the next subsection by comparing with alternative barrier regimes, this behavior is closely connected to the interplay between the vibrational decoherence and the surface crossing dynamics represented by the $\bar{Q}_{2x}(t)$ oscillation.

The total population decay of the locally excited P*B_L state

$$N(t) = N(0)\exp\left(-\int_0^t d\tau\ k_{ET}(\tau)\right) \qquad (24)$$

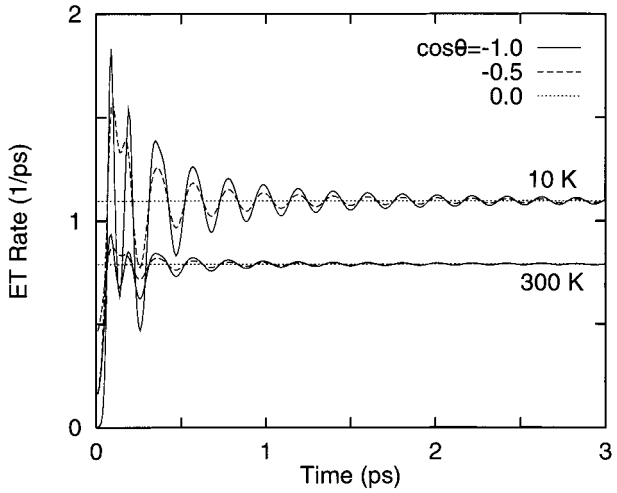

Figure 2. The time-dependent electron transfer rate $k_{ET}(t)$ at high (300 K) and low (10 K) temperatures calculated with the parameters for the bacterial photosynthetic primary ET. The solid, dashed, and dashed−dotted curves correspond to cos $\theta = -1$, -0.5, and 0, respectively.

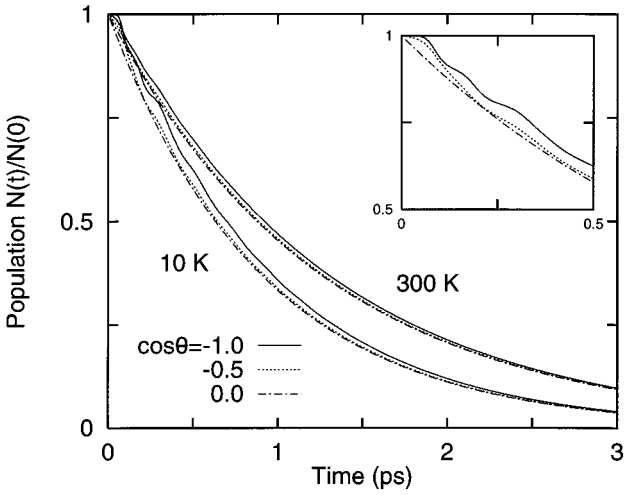

Figure 3. The (normalized) population decay $N(t)/N(0)$ of the locally excited P* state calculated from the time-dependent rate $k_{ET}(t)$ in Figure 2. The inset is a magnification of the short-time region of the low-temperature (10 K) case.

is plotted in Figure 3. We consider that $N(t)$ is of principal relevance to the study of the vibrational coherence effects on the nonequilibrium ET rate and mechanism. On the other hand, the recent experimental works[4] yielded time-resolved luminescence intensities at several probing wavelengths, which reflect the transient evolution of the population at the corresponding Franck−Condon energies. Thus, the approximate correspondence to $N(t)$ would be obtained by integrating those data over the relevant wavelength region.

As seen in Figure 3, the oscillation in $N(t)$ is rather small despite of the marked oscillation seen in $k_{ET}(t)$. The whole decay profile depends primarily on the temperature rather than on the angle θ. Although it might require very high resolution of data, it would be possible to obtain $k_{ET}(t)$ experimentally by taking the time derivative of the measured $N(t)$.

The computed results semiquantitatively reproduce the anomalous temperature dependence (accelerated as temperature decreases) of the bacterial primary ET rate. Interestingly, this is true irrespective of the angle θ, even including the orthogonal case (cos $\theta = 0$). This implies that the temperature anomaly is not quite relevant to the nonequilibrium vibrational coherence in the P* state.

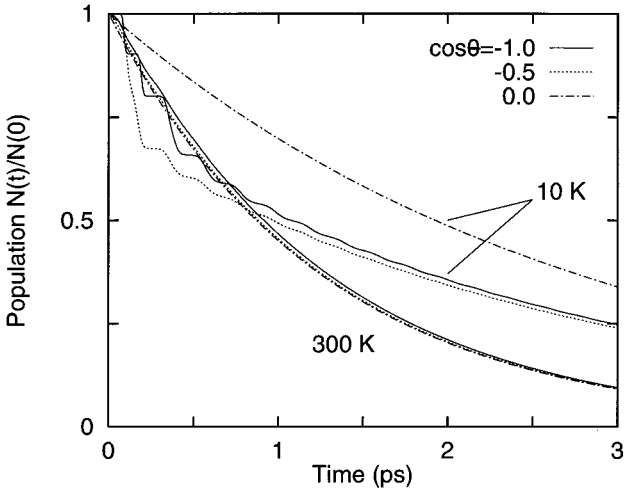

Figure 4. Same as Figure 3 but calculated with the classical limit ($\beta\hbar\omega \rightarrow 0$) of the parameters Λ and Γ.

One plausible origin for the temperature dependence would be the static energetic arrangement of the system that gives small barrier for the ET process. Indeed, the (classical) activation barrier for the ET, given by $\Delta^2/4(\lambda_x' + \lambda_y)$, is only 14 cm^{-1} for the parameters employed here. As discussed in the next subsection, qualitatively similar behavior of the population decay is seen for the barrierless case.

Another possibly important factor for elucidating the temperature dependence would be the nuclear tunneling effects that may be dominant at low temperature. To examine this, we tentatively put the classical limt $\beta\hbar\omega \rightarrow 0$ of Λ and Γ in eq 20 and compute $N(t)$. The results are displayed in Figure 4. As seen, the classical calculations for 300 K does not differ very much from the semiclassical ones in Figure 3. On the other hand, the discrepancy between the semiclassical and classical calculations is prominent at 10 K, which is due to the nuclear tunneling effects. The classical model does not reproduce the experimentally observed acceleration of the bacterial primary ET at lower temperatures.

Interestingly, Figure 4 also shows that the oscillation in $N(t)$ at 10 K is more remarkable in the classical calculations. This is rationalized from the values of Λ, the square root of which is the Gaussian width of $F_Q(t)$ in eq 11. The computed values of $\sqrt{\Lambda}$ at10 K are 410 cm^{-1} and 122 cm^{-1} for the semiclassical and classical cases, respectively. The difference is much smaller at 300 K: 775 cm^{-1} (semiclassical) and 764 cm^{-1} (classical). As noted in section II and in Appendix B, $F_Q(t)$ accounts for the surface crossing probability of the nuclear motion on the reaction coordinate $Q_2(t)$ broadened by the thermal distribution around its average motion $\bar{Q}_{2x}(t)$. The oscillation of $\bar{Q}_{2x}(t)$, which is temperature independent, is reflected more sharply in $k_{ET}(t)$ for the classical Λ at low temperature because the broadening is smaller.

To summarize, these results suggest that *both* the static energetics (that give small barrier) and the nuclear tunneling effects are the main origins of the anomalous temperature dependence of the bacterial primary ET rate.[34]

In Figure 5, the transient behavior of $\bar{Q}_{2x}(t)$ is displayed. (Precisely, $\bar{Q}_{2x}(t) - \Delta$ is plotted.) For the nonorthogonal cases of $\cos\theta \neq 0$, $\bar{Q}_{2x}(t) - \Delta$ passes zero twice in the short time ($t \leq 0.2$ ps) where the surface crossing takes place on the average motion on the reaction coordinate. We will come back to this point in the next subsection.

B. Comparison with Other Parameter Regimes. The parameters assumed in the preceding subsection give rather small potential barrier for the ET process. Here we examine different barrier regimes for the aim to illuminate by comparison the essential characteristics of the bacterial systems.

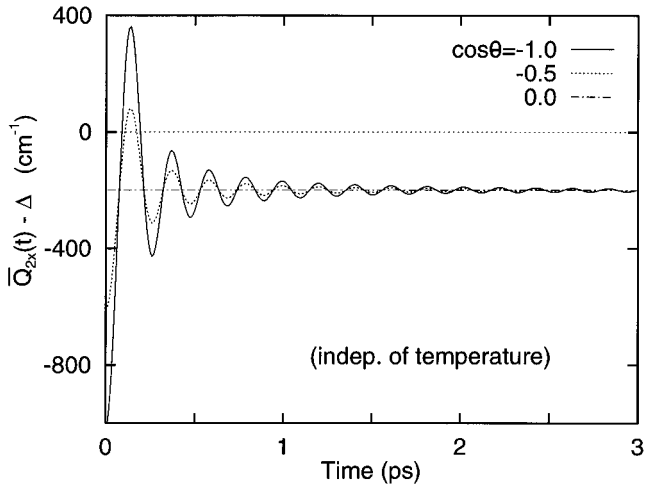

Figure 5. The average motion of the reaction coordinate $\bar{Q}_{2x}(t)$ (minus Δ) corresponding to the calculation of $k_{ET}(t)$ in Figure 2. (Note that $\bar{Q}_{2x}(t)$ is independent of the temperature.) The surface crossing on the average motion takes place at $\bar{Q}_{2x}(t) - \Delta = 0$.

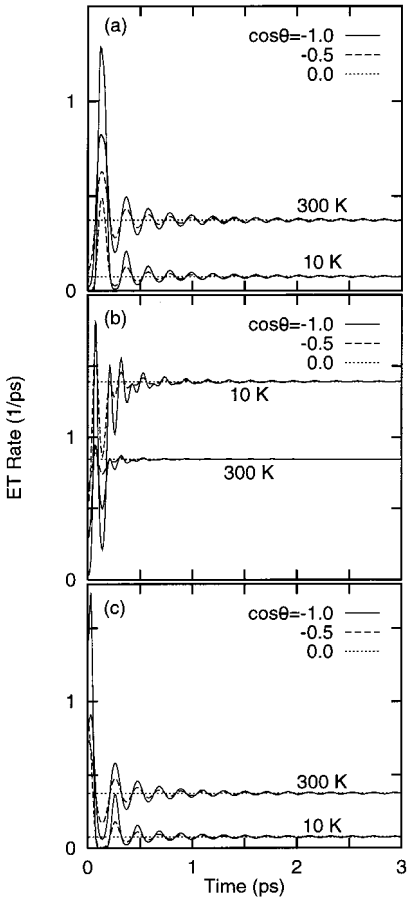

Figure 6. Same as Figure 2 but with varied energy gap parameter ϵ_3 for (a) thermoneutral $\epsilon_3 = 0$, (b) barrierless $\epsilon_3 = -(\lambda_x' + \lambda_y)$, and (c) inverted $\epsilon_3 = -2(\lambda_x' + \lambda_y)$ cases.

In Figures 6 and 7, we compare three cases of $k_{ET}(t)$ and $N(t)$: (a) thermoneutral $\epsilon_3 = 0$, (b) barrierless $\epsilon_3 = -(\lambda_x' + \lambda_y)$ and (c) inverted $\epsilon_3 = -2(\lambda_x' + \lambda_y)$. As seen, the oscillation period of $k_{ET}(t)$ is ~0.2 ps for parts a and c of Figure 6, which is in accord with that of $\bar{Q}_{2x}(t)$. On the other hand, the period for b is about half of them. The behavior of $\bar{Q}_{2x}(t)$ is identical among

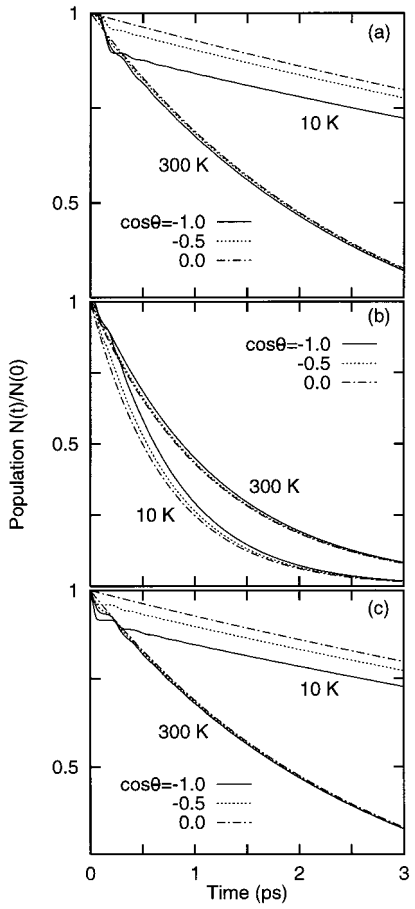

Figure 7. The (normalized) population decay $N(t)/N(0)$ of the locally excited state calculated from $k_{ET}(t)$ of Figures 6a−c.

a−c and the bacterial case shown in Figure 5, except that the location of the crossing condition on the average motion, $\bar{Q}_{2x}(t) - \Delta = 0$, is shifted. Between a and c the phase of the oscillation is almost inverted, which is due to the different location of the initial population relative to the surface crossing. As noted above, the oscillation frequency in b is almost twice as large as those in a and c. This is because the surface crossing event occurs twice in an oscillation period at the bottom of the potential well in the barrierless case b. On the other hand, for a and c with the nonnegligible barriers, the average motion on the reaction coordinate approaches the crossing region only once in an oscillation.

In comparison to these, the bacterial case with the small barrier examined in section III.A. is in an intermediate between a and b. In this case, the average motion passes the crossing in the very early stage as seen in Figure 5, resulting in the higher frequency oscillation of $k_{ET}(t)$ in the corresponding time region of Figure 2. As the oscillation of $\bar{Q}_{2x}(t)$ is damped due to dephasing, the average motion does not pass the surface crossing any more but only approach it, which result in the lower frequency oscillation of $k_{ET}(t)$ similarly to the case a.

These demonstrate that the transient behavior of the time-dependent ET rate carries useful information on the dynamical interplay between the dephasing and the surface crossing of the ultrafast reactions, which in turn reflects the underlying static energetics of the system.

The corresponding population decays of the locally excited state for the cases a−c are plotted in Figure 7. The barrierless case b appears similar to the bacterial case in Figure 3, for both of them the population decay is faster at the lower temperature, and the overall features are rather insensitive to the marked

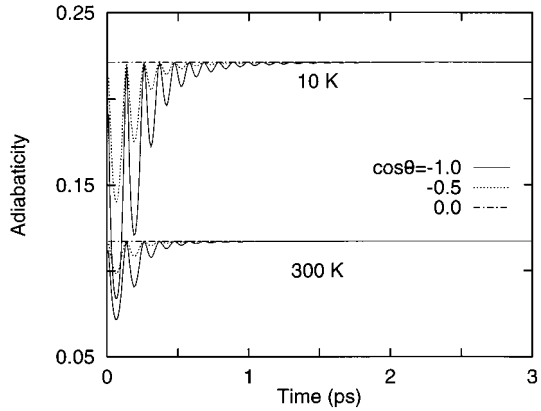

Figure 8. The adiabaticity parameter γ for the bacterial photosynthetic primary ET (corresponding to $k_{ET}(t)$ and $N(t)$ in Figures 2 and 3).

oscillation seen in $k_{ET}(t)$. In contrast, acceleration of the initial decay is clearly seen for cases a and c at the low temperature (10 K), which is most remarkable for the linear arrangement, $\cos\theta = -1$. This implies that the nonequilibrium nuclear coherence may accelerate the transition when the barrier is nonnegligible (so that the vibrational motion may assist the surface crossing dynamics while the thermal activation is not efficient) and when the coherent vibration can directly (i.e., $\cos\theta \simeq \pm 1$) access the crossing region. However, these conditions do not seem to apply for the bacterial primary ET as discussed in section III.A., for which the nonequilibrium nuclear vibrations are seen to be almost irrelevant to the total population decay rate.

C. Adiabaticity and the Applicability of the Landau−Zener Formula. In the theories of Landau−Zener type, the adiabaticity of the electronic transition is usefully measured by

$$\gamma \equiv \frac{2\pi J^2}{\hbar v}\begin{cases}\gamma \ll 1 & \text{nonadiabatic}\\ \gamma \gg 1 & \text{adiabatic}\end{cases} \tag{25}$$

Here we define the effective velocity v by

$$v(t)^2 \equiv \sqrt{\frac{1}{\pi\Gamma}}\int_{-\infty}^{\infty} dP\, e^{-P^2/\Gamma}\,(\dot{\bar{Q}}_{2x}(t) + P)^2 = \dot{\bar{Q}}_{2x}(t)^2 + \frac{\Gamma}{2} \tag{26}$$

as a time-dependent quantity.

In order for the Landau-Zener formula to be adequate for the condensed phase reactions, it is required that $v(t)$ does not undergo significant variation during the passage through the transition region. From considerations that follow ref 20, we have checked that the use of the Landau−Zener formula is adequate for the present system, since $v(t)$ does not vanish because of $\Gamma/2$ in eq 26 even when the velocity $\dot{\bar{Q}}_{2x}(t)$ of the average motion vanishes. Therefore, the Landau−Zener formula is applicable even at the turning point of the $\bar{Q}_{2x}(t)$ path or in the long-time steady-state region. Especially, the small barrier assumed for the bacterial RCs is preferable for the Landau−Zener formula as it raises the chance of ballistic passage through the transition region.

Figure 8 shows the computed adiabaticity γ for the bacterial ET as examined in section III.A. At each temperature, the upper limit is given by the orthogonal case, $\cos\theta = 0$, in which $k_{ET}(t)$ and other quantities are independent of the nonequilibrium vibrational coherence. Namely, the extra momentum caused by the nonequilibrium vibrations suppresses the adiabaticity because of nonvanishing $\dot{\bar{Q}}_{2x}(t)$ in eq 26. This effect is less drastic at higher temperature because it is thermally masked by a larger

Γ in eq 26. (See also the discussion pertaining to the nuclear tunneling effects in section III.A.) The adiabaticity is larger at the lower temperature because Γ decreases in eq 26. In both high and low temperatures, γ is not very large (≤ 0.25). We estimated that the electronic coupling J should be as large as 100 and 75 cm^{-1} at 300 and 10 K, respectively, in order that $\gamma \simeq 1$.

IV. Conclusion

We have developed a theory to describe nonequilibrium electronic surface-crossing processes induced by ultrafast photoexcitations. Our time-dependent transition rate $k_{ET}(t)$ essentially includes, as its perturbational (small electronic coupling) limit, the formula derived by Cho and Silbey.[17] Furthermore, the steady-state (long-time) limit of this perturbational form reduces to the well-known "semiclassical" or "static" ET rate.[35]

One of the novel key concepts exploited here is the angle between the two microscopic reaction coordinates, one for describing the nonequilibrium dynamics induced by the photoexcitation and the other for the ET process. The vibrational coherence and its dephasing are described in terms of the average motion on the reaction coordinate $\bar{Q}_{2x}(t)$, which determines the time-dependent ET rate in the course of its damped oscillation. The cross-spectral density function $c(\omega)$ is another key quantity introduced here, which represents the direction cosine of the angle between the two reaction coordinates.

Numerical calculations are performed with parameters for the primary ET in bacterial photosynthetic RCs and for related (thought) systems of various static barrier regimes. The pictures emerged from the calculations are summarized as follows: (1) the nonequilibrium nuclear vibrations induced by photoexcitation may accelerate the subsequent electronic transitions in cases where (i) the temperature is low, (ii) $\cos\theta \simeq \pm 1$ (i.e., the linear arrangement) so that the average motion on the reaction coordinate may directly realize the surface crossing, and (iii) there is a significant barrier for the electronic transition so that the reaction via thermal activation is not very efficient. However, the conditions ii and iii do not seem to apply for the bacterial primary ET. Especially, the linear arrangement of the two reaction coordinates is not plausible because of the heterogeneity of the environment around the chromophores in the bacterial RCs as explained in Introduction. Also, the experimentally found acceleration of the ET rate at lower temperature appears to be reproducible only with a rather small potential barrier. (See next.) (2) To the anomalous temperature dependence of the bacterial primary ET rate, the nonequilibrium nuclear coherence in the P* state is not quite relevant. It is brought about by the static energy arrangement that gives small barrier for the ET step *and* the quantum nuclear tunneling effect at low temperature, as has already been discussed.[36] (3) When the barrier for the electronic transition exists but is not very high, the system may pass through the surface crossing twice an oscillation in the course of the nonequilibrium average motion on the reaction coordinate in the early stage after the photoexcitation. In the meanwhile, the average motion $\bar{Q}_{2x}(t)$ is damped due to dephasing among component bathh modes so that it no more passes but only approaches the crossing once an oscillation period. In this case, change of the oscillation period of the time-dependent rate $k_{ET}(t)$ may be observed. Namely, the oscillation frequency of $k_{ET}(t)$ may change reflecting the transient behavior of the interplay between the nuclear dephasing and the surface crossing dynamics. We propose that detailed experimental analysis[37] of this aspect may in turn provide useful information on the dynamical mechanism and underlying static energetics of ultrafast reactions. In the present model for the bacterial primary ET, the oscillation frequency of $k_{ET}(t)$ is around 240 cm^{-1} (in energy unit) in the initial stage within ~0.3 ps after the photoexcitation and then reduces to ~120 cm−1 as the dephasing proceeds. This is comprehended via the behavior of $\bar{Q}_{2x}(t)$ in Figure 5 around the surface crossing of the average motion on the reaction coordinate, $\bar{Q}_{2x}(t) - \Delta = 0$, in view of the picture sketched above.

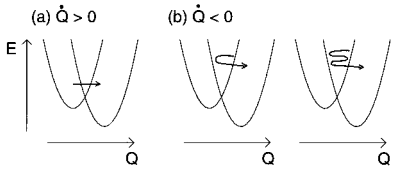

Figure 9. Schematic illustration of the two terms in the transmission coefficient $\kappa(\dot{Q})$ of eq 9, for (a) $\dot{Q} > 0$ and (b) $\dot{Q} < 0$.

Although we believe that the essential features of the bacterial primary ET are captured by the present model, it would be also intriguing to perform more realistic and detailed analysis with molecular simulation methods. To this end, the microscopic theory developed in section II will provide a useful basis.

Acknowledgment. Numerical calculations were carried out at Science Information Processing Center of the University of Tsukuba. We thank Professor Shuji Abe for useful comments. K.A. acknowledges support from the University of Tsukuba Research Projects and the Grants in Aid for Scientific Research from the Ministry of Education (Grant 09740415). He also thanks Professor Graham Fleming for pointing us to ref 17 at US/Japan Seminar (November, 1997) at which a part of this work was presented.

Appendix A: Transmission Coefficient $\kappa(\dot{Q})$

The form of $\kappa(\dot{Q})$ in eq 9 is schematically explained in Figure 9. When the system reaches the surface crossing region with $\dot{Q}_2 > 0$, the transition probability is given by P_{LZ} (Figure 9a). On the other hand, when $\dot{Q}_2 < 0$, the summation over the diagrams in Figure 9b

$$P_{LZ}(1 - P_{LZ}) + P_{LZ}^3(1 - P_{LZ}) + ... \qquad \text{(A.1)}$$

leads the second term in eq 9.

Appendix B: Derivation of Equation 11

Since the $\{y_j\}$ bath modes are not coupled to the photoexcitation in the present model, they remain in thermal equilibrium during the ET process. Thus, in the integration of eq 7, we can put $Q_{2y}(0)$ and $\dot{Q}_{2y}(0)$ in place of $Q_{2y}(t)$ and $\dot{Q}_{2y}(t)$ by assuming the ergodicity of the equilibrium variables. This simplifies and enables the $\{y_j\}$ integrations (as the variables are included only in $Q_{2y}(0)$ in the δ function).

For integration by the $\{x_i\}$ variables with the shifted Wigner distribution function of eq 8, we define $X_i \equiv x_i - \xi_i/\hbar\omega_i$ and rewrite $\bar{Q}_{2x}(t)$ as

$$Q_{2x}(t) = \bar{Q}_{2x}(t) + \sum_i \xi_i'(X_i \cos\omega_i t + p_i \sin\omega_i t)$$

$$\equiv \bar{Q}_{2x}(t) + \delta Q_{2x}(t) \qquad \text{(B.1)}$$

in which $\bar{Q}_{2x}(t)$ is defined by eq 12. This means that $\bar{Q}_{2x}(t)$ represents the "systematic" or "average" nuclear motion on the

TABLE 1: Various Forms of Cross-Spectral Density Function $c(\omega)$ and Corresponding $\bar{Q}_{2x}(t)$. See Appendix C for $n_{x',y}$ in the Last Column

$c(\omega)$	s	A	$\bar{Q}_{2x}(t)$	$n_{x',y}$
$A\omega^s\sqrt{\omega^2{}_c-\omega^2}$	1	$\frac{4\lambda_c}{\pi\omega_c^2}$	$\frac{4\lambda_c}{\omega_c t}J_1(\omega_c t)$	1/4
	3	$\frac{16\lambda_c}{\pi\omega_c^4}$	$\frac{16\lambda_c}{(\omega_c t)^2}\{\omega_c t J_1(\omega_c t) - 3J_2(\omega_c t)\}$	1/2
	5	$\frac{32\lambda_c}{\pi\omega_c^6}$	$\frac{32\lambda_c}{(\omega_c t)^4}\{\omega_c t J_3(\omega_c t) - 6(\omega_c t)^2 J_4(\omega_c t) + (\omega_c t)^3 J_5(\omega_c t)\}$	5/8
$A\omega^s e^{-\omega/\omega_C}$	1	$\frac{\lambda_c}{\omega_c}$	$\frac{2\lambda_c}{1+(\omega_c t)^2}$	2
	3	$\frac{\lambda_c}{2\omega_c^2}$	$\frac{2\lambda_c(1-3(\omega_c t)^2)}{(1+(\omega_c t)^2)^3}$	12
	5	$\frac{\lambda_c}{24\omega_c^5}$	$\frac{2\lambda_c(1-10(\omega_c t)^2+5(\omega_c t)^4)}{(1+(\omega_c t)^2)^5}$	30

reaction coordinate induced by the nonequilibrium distribution created at $t = 0$. The remainder denoted by $\delta Q_{2x}(t)$ describes the thermal fluctuation around $\bar{Q}_{2x}(t)$. Since the fluctuation in $\delta Q_{2x}(t)$ are also ergodic, the integration by $\{X_i\}$ can be done in a similar way as $\{y_j\}$, which gives $F_Q(t)$ in eq 11. Finally, by introducing a distribution function defined by

$$G(P) \equiv \int\int \mathrm{d}p_i\, \mathrm{d}p_j\, \tilde{W}(p_i)\tilde{W}(p_j)\delta(P - \delta\dot{Q}_{2x} - \dot{Q}_{2y}) \qquad \text{(B.2)}$$

in which $\tilde{W}(p)$ denotes the momentum part of the harmonic Wigner distribution function $W(p, x)$ and the integrations by $\{p_i\}$ and $\{p_j\}$ are reduced to a one-dimensional one such as

$$\int_{-\infty}^{\infty}\mathrm{d}P\; G(P)\kappa(\dot{\bar{Q}}_{2x}(t) + P)|\dot{\bar{Q}}_{2x}(t) + P| \qquad \text{(B.3)}$$

which gives $F_P(t)$ in eq 11.

Besides the straightforward derivation outlined above, it would be also useful to first consider that the thermal fluctuations in $Q_2(t)$ and $\dot{Q}_2(t)$ are statistically independent of each other at each time t. This means that eq 7 is factorized as $k_{ET}(t) = F_Q(t)F_P(t)$ with $F_Q(t) \equiv \langle\langle\delta(Q_2(t) - \Delta)\rangle\rangle_1$ and $F_P(t) \equiv \langle\langle\kappa(\dot{Q}_2(t))|\dot{Q}_2(t)|\rangle\rangle_1$, which leads eq 11.

Appendix C: Spectral Density Functions

As explained in section III, we consider the "superohmic" and "truncated" form of eq 21 is adequate for the cross-spectral density function $c(\omega)$ of the present system. However, it would be also useful to examine alternative forms for comparison and for various applications of the general theory developed in section II.

Table 1 summarizes several representative forms of $c(\omega)$ with corresponding $\bar{Q}_{2x}(t)$, including ohmic ($s = 1$) to superohmic ($s > 1$) and two types of the frequency cutoff. The prefactor A is determined from the sum relation eq 17. As seen, the exponential cutoff gives strongly damped decay of $\bar{Q}_{2x}(t)$ accompanying only a few weak oscillations for both the ohmic and superohmic cases. Thus, it might not be really adequate for systems such as the bacterial photosynthetic RCs that are found to exhibit vibrational coherence in ultrafast experiments. On the other hand, the square-root cutoff gives oscillatory $\bar{Q}_{2x}(t)$ as illustrated in Figure 5. Naturally, damping in $\bar{Q}_{2x}(t)$ is stronger for broader dispersion of $c(\omega)$.

The last column of Table 1 lists the number corresponding to n_x' or n_y in eq 14. By using the "ordinary" spectral density functions $\rho_{x'}(\omega)$ and $\rho_y(\omega)$, the classical limit ($\beta\hbar\omega \to 0$) of Γ in eq 13 is written as

$$\Gamma \to 4k_B T\{\int \mathrm{d}\omega\; \omega\rho_{x'}(\omega) + \int \mathrm{d}\omega\; \omega\rho_y(\omega)\} \qquad \text{(C.1)}$$

For the functional forms listed in Table 1, these integrals can be calculated to give n_x' and n_y in eq 14. In this case, $c(\omega)$, λ_c, and ω_c in Table 1 should read instead as $\rho_{x',y}(\omega)$, $\lambda_{x',y}$, and $\omega_{x',y}$.

References and Notes

(1) Woodbury, N. W.; Becker, M.; Middendorf, D.; Parson, W. W. *Biochemistry* **1985**, *24*, 7516.

(2) Martin, J.-L.; Breton, J.; Hoff, A. J.; Migus, A.; Antonetti, A. *Proc. Natl. Acad. Sci. U.S.A.* **1986**, *83*, 957.

(3) Fleming, G. R.; Martin, J.-L.; Breton, J. *Nature* **1988**, *333*, 190.

(4) Vos, M. H.; Rappaport, F.; Lambry, J.-C.; Breton, J.; Martin, J.-L. *Nature (London)* **1993**, *363*, 320. Vos, M. H.; Jones, M. R.; Hunter, C. N.; Breton, J.; Lambry, J.-C.; Martin, J.-L. *Biochemistry* **1994**, *33*, 6750.

(5) Stanley, R. J.; Boxer, S. G. *J. Phys. Chem.* **1995**, *99*, 859.

(6) Shreve, A. P.; Cherepy, N. J.; Franzen, S.; Boxer, S. G.; Mathies, R. A. *Proc. Natl. Acad. Sci. U.S.A.* **1991**, *88*, 11207. Cherepy, N. J.; Shreve, A. P.; Moore, L. J.; Franzen, S.; Boxer, S. G.; Mathies, R. A. *J. Phys. Chem.* **1994**, *98*, 6023.

(7) Middendorf, T. R.; Mazzola, L. T.; Gaul, D. F.; Schenck, C. C.; Boxer, S. G. *J. Phys. Chem.* **1991**, *95*, 10142. Lyle, P. A.; Kolaczkowski, S. V.; Small, G. J. *J. Phys. Chem.* **1993**, *97*, 6924.

(8) For example, *Ultrafast Reaction Dynamics and Solvent Effects: Theoretical and Experimental Aspects*; Gauduel, Y., Rossky, P. J., Eds.; AIP Press: New York, 1994. Zewail, A. H. *Femtochemistry: Ultrafast Dynamics of the Chemical Bond*; World Scientific: Singapore, 1994. Fleming, G. R.; Cho, M. *Annu. Rev. Phys. Chem.* **1996**, *47*, 109.

(9) Bradforth, S. E.; Jaminez, R.; van Mourik, F.; van Grondelle, R.; Fleming, G. R. *J. Phys. Chem.* **1995**, *99*, 16179. Chachisvillis, M.; Fidder, H.; Pullerits, T.; Sundström, V. *J. Raman Spectrosc.* **1995**, *26*, 513. Joo, T.; Jia, Y.; Yu, Y.-Y.; Jonas, D. M.; Fleming, G. R. *J. Phys. Chem.* **1996**, *100*, 2399.

(10) Wang, Q.; Schoenlein, R. W.; Peteanu, L. A.; Mathies, R. A.; Shank, C. V. *Science* **1994**, *266*, 422.

(11) For example, Sherer, N. F.; Jonas, D. M.; Fleming, G. R. *J. Chem. Phys.* **1993**, *99*, 153. Wynne, K.; Galli, C.; Hochstrasser, R. M. *J. Chem. Phys.* **1994**, *100*, 4797. Dhar, L.; Rogers, J. A.; Nelson, K. A. *Chem. Rev.* **1994**, *94*, 157.

(12) Jean, J. M.; Friesner, R. A.; Fleming, G. R. *J. Chem. Phys.* **1992**, *96*, 5827. Jean, J. M.; Fleming, G. R. *J. Chem. Phys.* **1995**, *103*, 2092.

(13) Lin, S. H.; Alden, R. G.; Hayashi, M.; Suzuki, S.; Murchison, H. A. *J. Phys. Chem.* **1993**, *97*, 12566.

(14) Coalson, R. D.; Evans, D. G.; Nitzan, A. *J. Chem. Phys.* **1994**, *101*, 436.

(15) Tanimura, Y.; Mukamel, S. *J. Chem. Phys.* **1994**, *101*, 3049.
(16) Kühn, O.; May, V.; Schreiber, M. *J. Chem. Phys.* **1994**, *101*, 10404.
(17) Cho, M.; Silbey, R. *J. Chem. Phys.* **1995**, *103*, 595.
(18) Kharkats, Y. I.; Kuznetsov, A. M.; Ulstrup, J. *J. Phys. Chem.* **1995**, *99*, 13545, 13555.
(19) For other theoretical studies on the equilibrium aspects of the bacterial primary ET, for example, see: Hu, Y.; Mukamel, S. *Chem. Phys. Lett.* **1989**, *160*, 410; *J. Chem. Phys.* **1989**, *91*, 6973. Bixon, M.; Jortner, J.; Michel-Beyerle, M. E. *Biochim. Biophys. Acta.* **1991**, *1056*, 301. Skourtis, S. S.; da Silva, A. J. R.; Bialek, W.; Onuchic, J. N. *J. Phys. Chem.* **1992**, *96*, 8034.
(20) Sumi, H. *J. Phys. Soc. Jpn.* **1982**, *51*, 1743.
(21) Sumi, H. *Phys. Rev. Lett.* **1983**, *50*, 1709; *J. Phys. C* **1984**, *17*, 6071.
(22) Sumi, H.; Kakitani, T. *Chem. Phys. Lett.* **1996**, *252*, 85.
(23) Sumi, H. *J. Electroanal. Chem.* **1997**, *438*, 11.
(24) Schmidt, S.; Arlt, T.; Hamm, P.; Huber, H.; Nägele, T.; Wachtveitl, J.; Meyer, M.; Scheer, H.; Zinth, W. *Chem. Phys. Lett.* **1994**, *223*, 116.
(25) For example, Feynman, R. P. *Statistical Mechanics: A Set of Lectures*; Addison-Wesley: Reading, 1972.
(26) Landau, L. D.; Lifshitz, E. M. *Quantum Mechanics*; Pergamon: Oxford, 1958. Zener, C. *Proc. R. Soc. London A* **1932**, *137*, 696; *Proc. R. Soc. London* **1933**, *140*, 660.
(27) It would be useful to specify other differences between Cho−Silbey's ET rate formula and the perturbational limit, eq 19, of ours. Their "time-dependent reorganization energy" and our $\bar{Q}_{2x}(t)$, both represent the key quantities, are apparently different from each other, as the former is always zero at $t = 0$ while the latter is generally not. The angle θ defined here appears to be equivalent to their "dimensionality parameter" although the conceptual viewpoint is quite different. Indeed, we consider that the connection between $\bar{Q}_{2x}(t)$ and θ via $c(\omega)$ is comprehensive and useful.
(28) Other differences from the present work include (1) the damping factors to the bath dynamics were introduced phenomenologically and (2) the aspect of the angle between the photoexcitation and the ET coordinates was not considered in ref 18.
(29) For example, Ando, K. *J. Chem. Phys.* **1994**, *101*, 2850; *J. Chem. Phys.* **1997**, *106*, 116; *J. Chem. Phys.* **1997**, *107*, 4585.
(30) Flynn, C. P.; Stoneham, A. M. *Phys. Rev.* **1970**, *B1*, 3966. Sethna, J. P. *Phys. Rev.* **1981**, *B24*, 698; *Phys. Rev.* **1982**, *B25*, 5050. Teichler, H.; Seeger, A. *Phys. Lett.* **1981**, *A82*, 91.
(31) The 120 cm^{-1} frequency is sometimes attributed to the interdimer motion of the special pair P because it is absent in the bacteriochlorophyll monomer. However, the possibility of assigning it to some environmental protein fluctuations does not seem to be ruled out.
(32) Nakagawa, H.; Okada, T.; Koyama, Y. *Biospectroscopy* **1995**, *1*, 169.
(33) Scherer, P. O. J.; Fischer, S. F. *Chem. Phys.* **1989**, *131*, 115. Scherer, P. O. J.; Scharnagl, C.; Fischer, S. F. *Chem. Phys.* **1995**, *197*, 333.
(34) For an alternative discussion which considers temperature dependence of ϵ_3 and λ due to the entropy effect, see: Kakitani, T.; Okada, A. In *Research in Photosynthesis*; Murata, N., Ed.; Kluwer: Netherlands, 1992; Vol. I, p 425.
(35) Marcus, R. A. *J. Chem. Phys.* **1956**, *24*, 966, 979; *Ann. Rev. Phys. Chem.* **1964**, *15*, 155. Ulstrup, J. *Charge Transfer Processes in Condensed Media*; Springer-Verlag: Berlin, 1979.
(36) This latter aspect has been extensively discussed in, e.g., Bixon, M.; Jortner, J. *Chem. Phys. Lett.* **1989**, *159*, 17, within the framework of the traditional theory for the steady-state rate constant. The point here would be that this picture remains valid with the present nonequilibrium generalization of the theory. Indeed, this nonequilibrium aspect was the major question raised by the experimental works in ref 4.
(37) For the bacterial RC, it might appear that the quantum beat of the fluorescence from the P* state masks this aspect. As analyzed in ref 4, this fluorescence quantum beat reflects an oscillation of the P* population in the coordinate space of the nuclear motions during the vibrational thermalization. Its fluorescence energy is determined by the coordinate value. Therefore, after integrating the fluorescence intensity over its energy, we could obtain the total population decay whose oscillation comes only from the nonequilibrium ET in the course of the nuclear vibrational thermalization. Alternatively, the product state of the ET could be detected at different energy regions of the probe light. Then, time-resolved detection of its rise by the ultrafast pump-probe technique would give the oscillation of the population not masked by the fluorescence quantum beat.